AUT Journal of Electrical Engineering
10.22060/EEJ.2026.25521.5948

Advanced Solar Grid Integration Solution Using a High-Efficiency Coupled Inductor Multiport Converter for Optimized Power Delivery

Tappeta Amar Kiran[1*], Dondapati Ravi Kishore[2], Kosana Bhargava Rama Chinna Vyshnav[3], Thorati Ajay Bhargav[4], Mahanthi Aahaj Varun[5]

[1]Assistant Professor, Department of Electrical and Electronics Engineering, Godavari Institute of Engineering and Technology (A), Rajahmundry.
[2]Professor, Department of Electrical and Electronics Engineering, Godavari Global University, Rajahmundry.
[3,4,5]UG Scholar, Department of Electrical and Electronics Engineering, Godavari Institute of Engineering and Technology (A), Rajahmundry.

[1*]Corresponding author email: tappetaamarkiran@gmail.com

Abstract:

Currently, Photovoltaic (PV) solar power generation is integrated into distributed generation (DG) systems is becoming popular. Therefore, this research proposes a unique Coupled inductor based multiport (CIM) converter that combines battery storage and solar PV in a grid-connected system. The PV system produces inferior voltage owing to its intermittent and sporadic nature due to the climatic conditions. A CIM converter is utilized to convert the PV output voltage to the highest level. In order to combat the intermittency and instability associated with PV, a Proportional Integral (PI) controller is added to the grid to ensure a stable and uninterrupted supply of power. Also, the battery is exploited to store surplus energy from PV systems, permitting to use this stowed energy when the panels aren't producing electricity. A Three phase Voltage Source Inverter (3ϕ VSI) is used to transform steady DC to AC voltage and a LC filter is employed to lessen harmonics. Additionally, the grid voltage synchronization is carried out by PI controller on load side. The developed system is also tested with the simulation outcomes from MATLAB/Simulink and comparison is made with conventional approaches. The obtained outcomes show that it attains the efficiency of 97.46%, ensures the optimized power is delivered to the grid.

Keywords:

PV systems, CIM converter, PI controller, Battery, 3ϕ VSI.

1. Introduction

The main issue confronting current power system networks is greenhouse gas emissions from burning coal and fossil fuels, which contribute to global warming. Therefore, a smart power generating system that is environmentally safe and effective is needed [1-3]. Utilizing RES is essential to reducing the environmental effect of fossil fuels and finding alternative energy sources [4-5]. Since renewable energy technologies greatly increase global power production while emitting less greenhouse gases, they provides excellent solution [6, 7].Furthermore, when RESs are used, positive outcomes like a decrease in global warming and carbon dioxide emissions have been noted [8, 9].The current power generating design for clean and green energy incorporates Renewable Energy Sources (RES) like WT, ultra-capacitor, PV, FC, geothermal, etc. [10–12]. Among grid integrated RE technologies, solar PV systems are prevalent owing to its long lifespan, simplicity of installation, rooftop applications, abundant, lack of moving parts, clean energy production and free energy generation and low maintenance [13–16]. Subsequently, PV systems are inexpensive, quiet, abundant, and clean energy sources, but small efficiency, flexible PV output power from sporadic irradiance, and temperature make grid integration difficult [17]. This issues are overcome by using converters and some of the conventional types of converters are explained.

A Boost converter with low switch stress, great voltage gain, and the capacity to lower input-current and capacitor voltage ripple is developed in [18, 19] for solar PV systems. Due to their great efficiency, boost converters reduce the amount of energy lost during conversion. They operate at lower duty cycles, which lessen component stress and increase dependability. However, with high input current values (i.e., solar radiation), its efficiency drastically decreases. A Buck-Boost converter is presented in [20, 21]. By adding an additional inductor to the drain of the switch on the buck-boost converter, a better voltage conversion ratio is attained. However, the converter's transfer function has a right-half-plane zero, which complicates stabilization and adds control complexity. Cuk converters, which have a greater capacity for boosting and lessen the voltage stress on the switch, are developed in [22]. It is better to use this converter because of its

superior bidirectional current and voltage management capabilities. Great voltage gain and small voltage stress, enable the selection of an active switch, a lower on-state resistance and voltage rating, single switch operation and great efficiency are only a few of the benefits of the CIM converters. Nevertheless, the converter necessitates extra parts, such as an additional inductor and capacitor, which increases the circuit's complexity and cost. Hence, this research implements a CIM converter for enhancing the PV voltage. The key goals are,

- To enhance the PV voltage, a CIM converter is exploited.
- To stowe excess energy from PV system, battery is used, which acts as another input of CIM converter.

2. Proposed Methodology

Solar PV electricity is a pollution-free power source that enhances power quality and dependability while lessening the load on the central grid that is utilized extensively to meet energy demands. This paper proposes an advanced solar grid integration using a CIM converter for power quality enhancement.

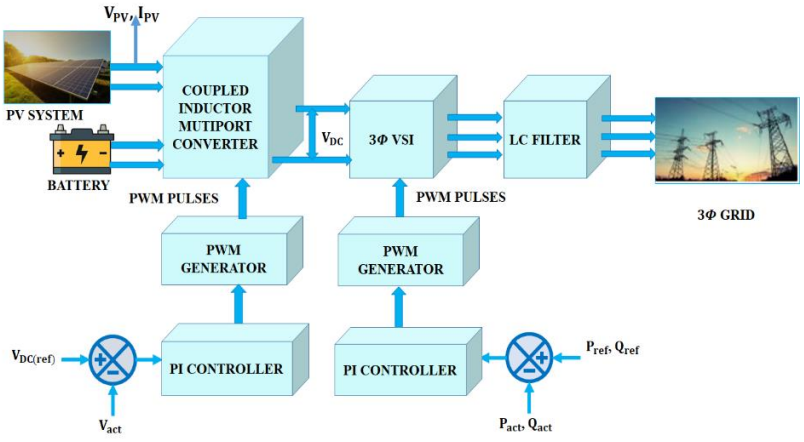

Fig. 1. Block diagram of advanced solar grid integration

Fig. 1 illustrates the block diagram of developed work. The CIM converter is employed to boost PV voltage. The battery is utilized to store excess energy, which is also an input of CIM converter. The PV system's

voltage is not stable so PI controller is utilized to alleviate the voltage. Then, the PWM generator produce pulses for CIM converter's superior switching function. After that, the DC link voltage is distributed to the 3ϕ VSI, transforms the DC into AC supply. The PI controller is exploited to control the inverter's function and PWM generator is utilized to control the switching operation of inverter. After that, the supply is subjected to grid with the help of LC filter, which removes the harmonics presented in the supply, assures the optimized power is delivered to the grid.

2-1- PV System

The PV system transmutes solar energy into electrical power, has served as the architectural basis of PV systems. A PV array is represented by a number of comparable circuits, but owing to its accuracy and simplicity, the single-diode circuit is the extensively employed. To demonstrate power losses, the circuit in Fig. 2 parallels a single diode with a photo-generated regulated current source and combines series and parallel resistance.

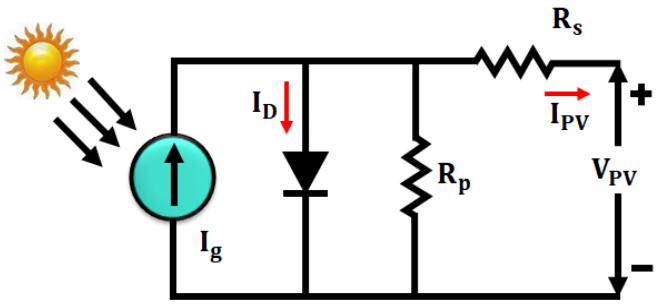

Fig. 2. Equivalent circuit of PV model

The development of the solar cell is based on P–N junctions, which are produced by semiconductor materials. Silicon is generally used because of its availability, non-toxicity, high and stable cell efficiencies, and stability. The implicit and nonlinear equations that follow yield the PV cell's I–V characteristics:

$$I_g - I_d - \left(\frac{V_{PV} + R_S I_{PV}}{R_P}\right) = I_{PV} \tag{1}$$

10.22060/EEJ.2026.25521.5948

$$I_O\left[exp\left(\frac{q\left(V_{PV}+R_S I_{PV}\right)}{nKT}\right)-1\right]=I_d \tag{2}$$

$$V_D = V_{PV} + R_S I_{PV} \tag{3}$$

Within an array, PV modules are connected in parallel and series. PV cells are attached in series to form strings, which are paired with more strings to form arrays. The current-voltage relationship of the array indicates these linkages, which are denoted by,

$$I_{PV} = N_P I_g - N_P I_d - \left(\frac{V_{PV}+\frac{N_S}{N_P}R_S I_{PV}}{\frac{N_S}{N_P}R_P}\right) \tag{4}$$

$$I_d = I_O\left[exp\left(\frac{q\left(V_{PV}+\frac{N_S}{N_P}R_S I_{PV}\right)}{N_S nKT}\right)-1\right] \tag{5}$$

The Boltzmann constant (K), idle factor (n), electron charge (q), irradiance current (I_g), diode saturation current (I_O), series and shunt resistance (R_S and R_P), series and parallel connection of strings (N_S and N_P), and output current and voltage of PV array ($I_{PV}$and V_{PV}) are all represented in the above expression. The PV system's low voltage is then subjected into a CIM converter, which enhances the voltage of PV system.

2-2- Coupled Inductor-Three Port Converter

The CIM converter is implemented, as shown in Fig. 3. A battery's voltage is represented by V_B, whereas the PV voltage is represented by V_{PV}. To clamp the voltage stress on the active switches and reuse the energy stowed in the leakage inductance, the capacitor C_3 is necessary.

10.22060/EEJ.2026.25521.5948

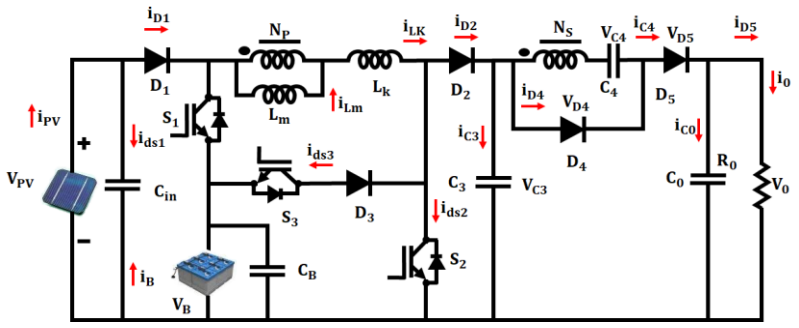

Fig. 3. Coupled inductor based three port converter

The additional voltage gain is produced by the secondary-side-coupled inductor N_S, diode D_4, capacitor C_4, and additional switching capacitor circuit. At this pointV_B, and V_{PV} supply energy to the load. S_1 and S_2 are the converter's main switches; $S_3$is typically off. The CIM converter's battery port functions as a bidirectional stage, with the duty ratio and phase relationship of the switches managing power flow. Surplus PV power increases the DC-link voltage during charging, the converter functions in buck stage, managing battery current and then voltage by feedback from measured battery current and voltage after the controller produces a positive current reference. When PV power is inadequate during draining, the converter functions in boost stage, supplying energy from the battery to sustain the DC connection and the controller reverses the current reference. A PI controller that tracks the reference current by modifying the duty cycle is employed to attain bidirectional current control, ensuring a seamless transition among charge and discharge stages. To impose limitations and safeguard the battery from overcurrent or deep discharge, current polarity and magnitude are unceasingly monitored. This system continues DC-link stability and effective power flow though ensuring smooth energy balancing between PV, battery and grid.

Here, $S_3$is actively gated in a CIM converter to enable power transfer rather than remaining off all the time. In actuality, $S_3$is stimulated by controller command to generate the energy transfer path via the coupled inductor among the PV and the battery port. When PV power surpasses load

10.22060/EEJ.2026.25521.5948

demand, the controller modulates S_3increases the duty ratio of the PV-side switch, producing the converter to run in buck stage and direct current into the battery. Therefore, rather of using a static normally off status of S_3, battery charging from PV is proficient by managed switching action and duty-cycle management.

Stage I (t_0 *to* t_1):

The maximum gain value is attained by V_{gs1} and V_{gs2} while $i_{Lm} > 0, i_{Lk} > 0$ and $i_{Lm} > i_{Lk}$ are present. Meanwhile V_B beats V_{PV} and D_1 is inactive. V_B provides energy to L_k. L_m, V_{C3} and V_{C4} provides the load with energy. This stage is ended if $i_{Lk} = i_{Lm}$ on period t_1, as displayed in Fig. 4.

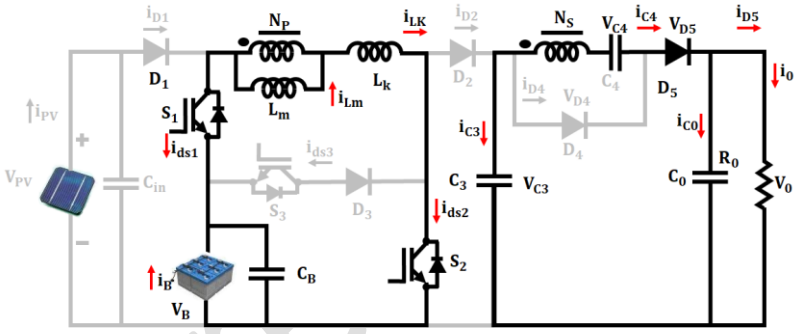

Fig. 4. Stage 1 of CIM converter

Stage II(t_1 *to* t_2):

V_{gs1} and V_{gs2} are highest with$i_{Lk} > 0, i_{Lm} > 0$ and $i_{Lm} = i_{Lk}$. V_B gives the energy to L_k and L_m that produce a linear rise on i_{Lk} and i_{Lm}. The components D_4, C_4, VC_4 and N_S generate the circuit of switched capacitor. This stage is ended while V_{gs1} is small (on period t_2). Fig. 5 represents the circuit diagram of Stage 2.

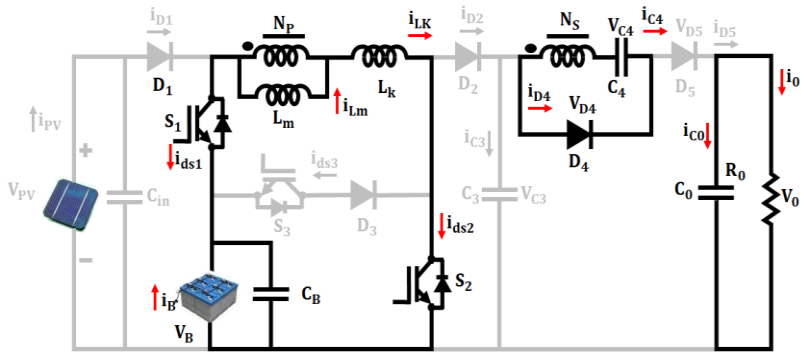

Fig. 5. Stage 2 of CIM converter

Stage III(t_2 *to* t_3):

$i_{Lm} > 0, i_{Lk} > 0,$ V_{gs1} and $i_{Lk} = i_{Lm}$ are small if V_{gs2} is maximum, as shown in Fig. 6 . The linear rise on i_{Lk} and i_{Lm} are produced by V_{in}, which provides the energy to L_k and L_m. This stage is ended while V_{gs2} (on period t_3) is small.

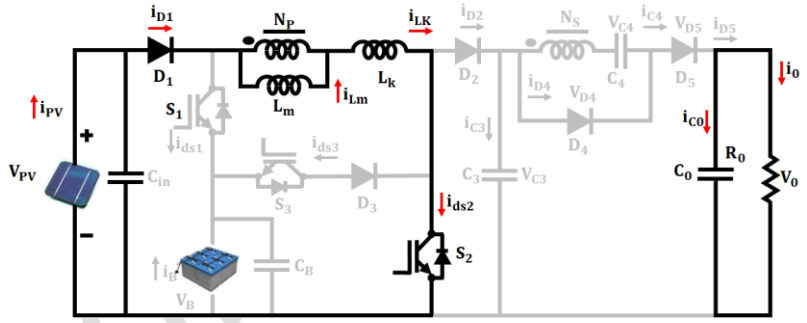

Fig. 6. Stage 3 of CIM converter

Stage IV (t_3 *to* t_4)

V_{gs2} and V_{gs1} are small. As an outcome of i_{Lk} charging, the capacitor at output C_{oss2} of S_2, V_{ds2} improves. This stage is finished $V_{ds2} = V_{C3}$ at period t_4. The circuit of stage 4 is presented in Fig. 7.

10.22060/EEJ.2026.25521.5948

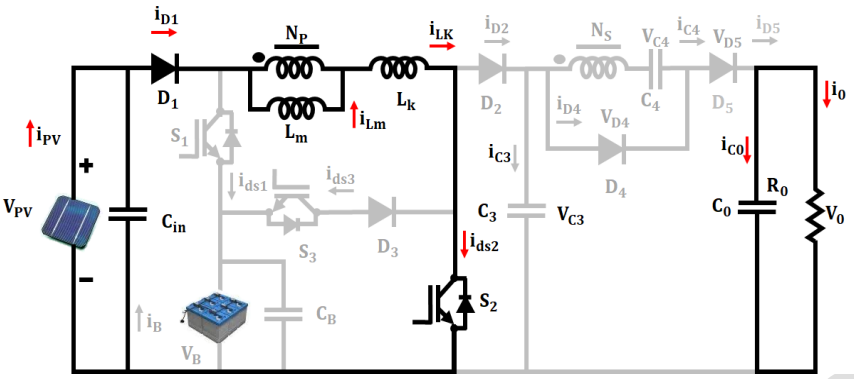

Fig. 7. Stage 4 of CIM converter

Stage V (t_4 *to* t_5)

V_{gs2} and V_{gs1} are small, as presented in Fig. 8. It reduces linearly because $i_{Lm} > 0$. The V_{C3} locksV_{ds2}. V_{in} and L_m provides the energy to capacitor C_3. V_{C3}, V_{C4} and L_m delivers the load with energy. If V_{gs1} and V_{gs2} are maximum at time t_5 this stage is finished.

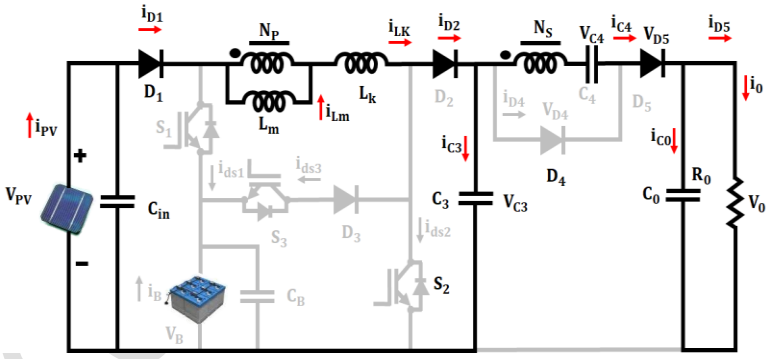

Fig. 8. Stage 5 of CIM converter

If S_1 and S_2 are active,

$$V_{Lm} = V_B \tag{6}$$

$$V_{Ns} = n, V_B = V_{C4} \tag{7}$$

10.22060/EEJ.2026.25521.5948

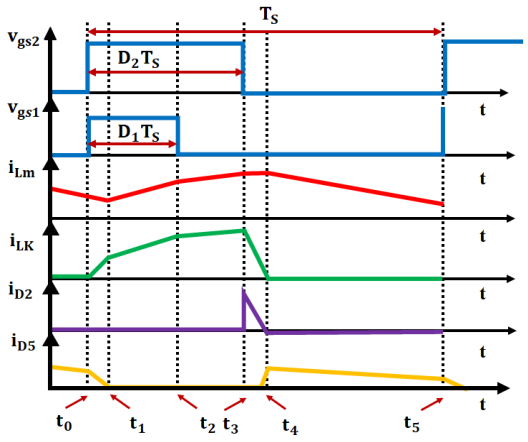

Fig. 9. Waveform of CIM converter

If S_1 is off and S_2 is active,

$$V_{Lm} = V_{in} \tag{8}$$

If S_1 and S_2 are inactive,

$$V_{Lm} = \frac{V_{in} + nV_B - V_O}{n+1} \tag{9}$$

The magnetic inductor L_m volt–balance principle is applied then the voltage gain

$$V_O = \frac{V_{in} + nV_B + (V_B - V_{in})(nD_1 - nD_2 + D_1)}{1 - D_2} \tag{10}$$

The waveform of CIM converter is presented in Fig. 9. The voltage of PV system is intermittent in nature so PI controller is applied to stabilize the voltage.

2-3- PI Controller

The incorporation of Integral controller (I) and Proportional controller (P) makes the PI controller. Fig. 10 reveals the PI controller's structure. It is made of reference signal, $R(s)$ and system's transferring signal $G_c(s)$ and $G_p(s)$. The PI controller's theoretic function is expressed in Equation (11)

$$G_c(s)\big|_{PI} = K_p + \frac{K_i}{S} = \frac{K_p S + K_i}{S} \tag{11}$$

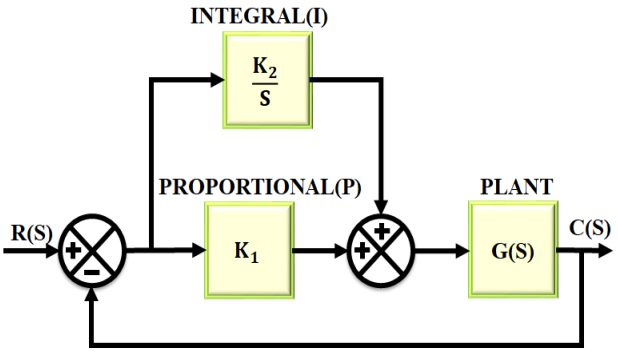

Fig. 10. PI controlling system

A PI controller processes the error that outcomes from linking the measured DC-link voltage with V_{dc}^{ref} to generate a reference current for the coupled-inductor stage. To prevent noise and guarantee precise regulation, the DC voltage feedback essentials to be appropriately filtered and scaled. Frequently, bandwidth separation is used, which places the voltage loop bandwidth considerably below the switching frequency and inner current dynamics. While the integral gain eradicates steady-state error but necessities to be forced to preserve stability margins, the proportional gain predicts response speed. After mapping this control output to a duty cycle, the PWM generator transforms it into gate pulses for the switches. PWM modulation depth and dynamics are directly impacted by loop adjustments, excessively aggressive tuning outcomes in duty ratio oscillations, whereas cautious tuning generates slower transient response. The benefits of PI controller are a lesser amount of stable errors and quicker response times. Subsequently, the grid synchronization by PI controller is discussed below.

2-4- ID Synchronization Using PI Controller

Grid synchronization is the process of supporting RESs' voltage, phase and frequency into line with the grid. Fig. 11 shows the current control method based on dq-PLL that is used to regulate VSI and accomplish grid voltage synchronization. By monitoring the grid voltage angle, the PLL makes that the inverter output is in phase with the grid. In order to simplify control in VSI, three-phase quantities are transformed into d and q components using the dq-axis transformation. The voltage and current in the dq frame are controlled by PI controllers. The equations for the system are

$$V_{in} = L_f * \frac{di}{dt} + R_f * i + V_{pcc} \tag{12}$$

$$L_f * \frac{di}{dt} = V_{in} - V_{pcc} + R_f * i \tag{13}$$

By applying Clark and Park transformation matrix,

$$\begin{pmatrix} i_d \\ i_q \end{pmatrix}^* = \frac{R}{L_f} * \begin{pmatrix} i_d \\ i_q \end{pmatrix} + \frac{1}{L_f} * \begin{pmatrix} V_{in\,d} - V_{pcc\,d} \\ V_{in\,q} - V_{pcc\,q} \end{pmatrix} + \omega \begin{pmatrix} i_q \\ -i_d \end{pmatrix} \tag{14}$$

$$\begin{pmatrix} u_{dass} \\ u_{qass} \end{pmatrix} = \omega * L_f * \begin{pmatrix} i_q \\ -i_d \end{pmatrix} + \begin{pmatrix} V_{in_d} - V_{pcc_d} \\ V_{in_q} - V_{pcc_q} \end{pmatrix} \tag{15}$$

$$\begin{pmatrix} u_{dass} \\ u_{qass} \end{pmatrix} = L_f * \begin{pmatrix} i_d \\ i_q \end{pmatrix}^* + R_f * \begin{pmatrix} i_d \\ i_q \end{pmatrix} \tag{16}$$

In s-domain the expression is

$$\begin{pmatrix} u_{dass} \\ u_{qass} \end{pmatrix}_{s-domain} = \left(L_f * S * R_f \right) * \begin{pmatrix} i_d \\ i_q \end{pmatrix}_{s-domain} \tag{17}$$

The d-q component's transfer function is

$$\begin{pmatrix} G_d \\ G_q \end{pmatrix} = \begin{pmatrix} \frac{i_d(s)}{u_{dass}(s)} \\ \frac{i_q(s)}{u_{qass}(s)} \end{pmatrix} = \begin{pmatrix} \frac{1}{S * L_f + R_f} \\ \frac{1}{S * L_f + R_f} \end{pmatrix} \tag{18}$$

10.22060/EEJ.2026.25521.5948

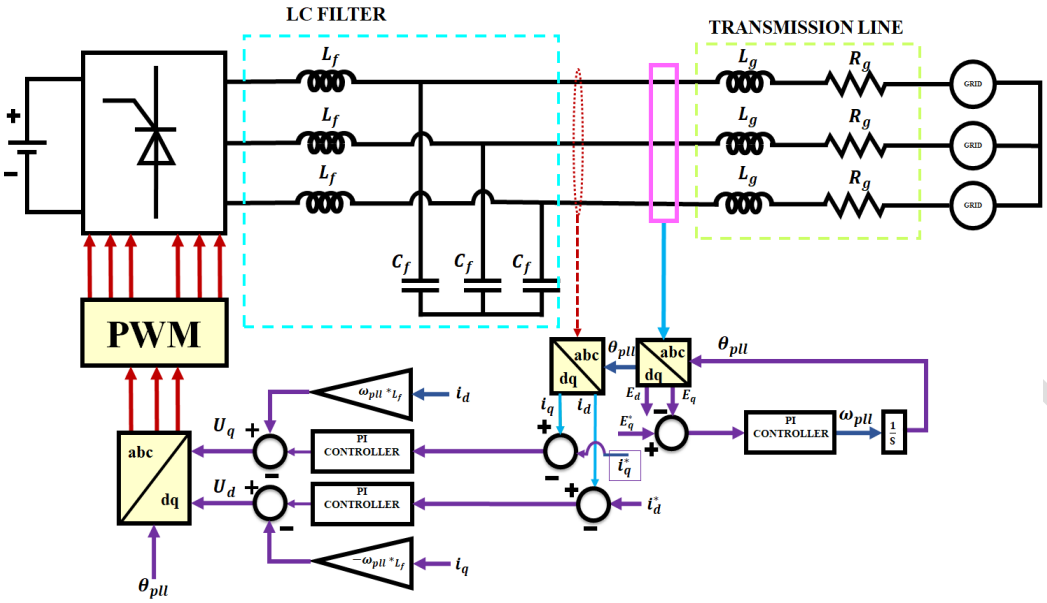

Fig. 11. Grid voltage synchronization

The current control loop is controlled by,

$$\begin{pmatrix} u_d \\ u_q \end{pmatrix} = \begin{pmatrix} k_{pd} e_d + k_{id} * \int e_d dt \\ k_{pq} e_q + k_{iq} * \int e_q dt \end{pmatrix} \tag{19}$$

$$\begin{pmatrix} e_d \\ e_q \end{pmatrix} = \begin{pmatrix} i_{dref} - i_d \\ i_{qref} - i_q \end{pmatrix} \tag{20}$$

The PI gains are,

$$K_p = \frac{2 * \zeta * \omega_c * L_f}{\sqrt{2 * \zeta^2 + 1 + \sqrt{\left(1 + 2 * \zeta^2\right)^2 + 1}}} \tag{21}$$

$$K_i = \left(\frac{\omega_c}{\sqrt{2 * \zeta^2 + 1 + \sqrt{\left(1 + 2 * \zeta^2\right)^2 + 1}}} \right)^2 * L_f \tag{22}$$

By regulating the reactive power's charge and discharge and adjusting the grid's frequency and phase, PI controllers ensure correct synchronization. Furthermore, the system is need to take grid impedance and other disturbances into consideration in order to guarantee small signal stability. Even with fluctuating load

and grid conditions, the smooth grid voltage synchronization is guaranteed by the precise tuning of the adaptive PLL gains and PI controller.

3. Results and Discussion

This section analyzes the waveforms of PV system with CIM converter in MATLAB/Simulink software. Subsequently, the comparison with conventional approaches are included in the section. The parameters of developed work is depicted in Table 1.

Table 1. Parameters of developed work

Parameter	Specification
PV System	
$Rated\ Power$	$10kW$
$Voltage\ (Open\ Circuit)$	$37.25V$
$Panels\ in\ series$	2
$Panels\ in\ Parallel$	32
$Current\ (Short\ Circuit)$	$8.95A$
CIM Converter	
C_B	$450\mu F$
$Switching\ frequency$	$10KHz$
D_1, D_2, D_3, D_4	MUR1560
C_O	$2200\mu F$

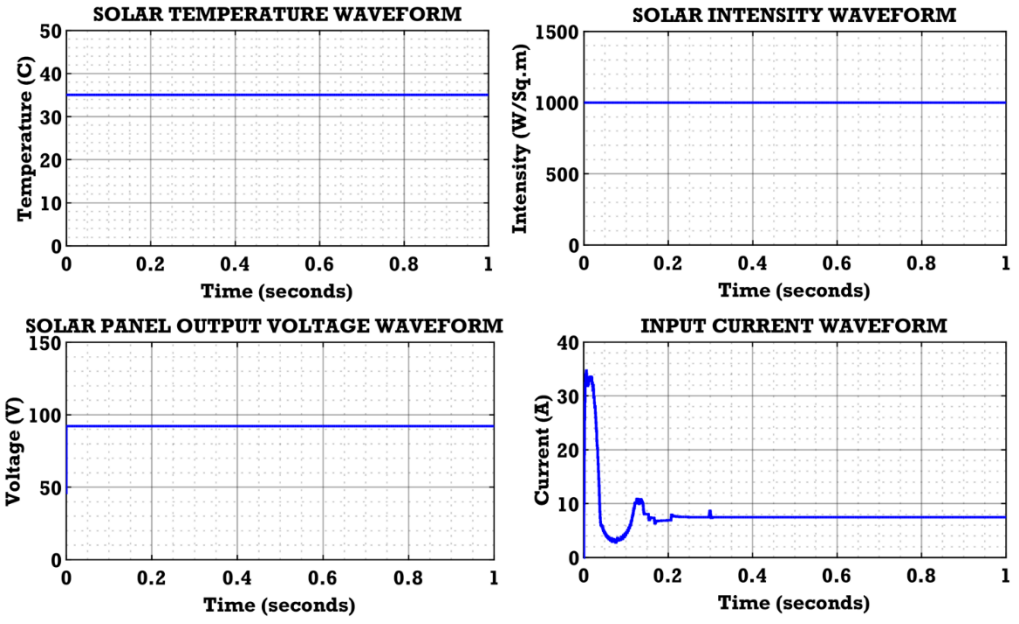

10.22060/EEJ.2026.25521.5948

Fig. 12. Waveform of solar panel

Fig. 12 illustrates the waveform of solar and the temperature is continued a steady value of 35℃ in the whole system. Likewise, the intensity is continued at $1000(W/Sq.m)$ all over the system. Based on these values, the voltage and current value is varied. In the entire system, the output voltage is continued at $90\ V$ and the input current is arbitrarily altered and continued at $8\ A$.

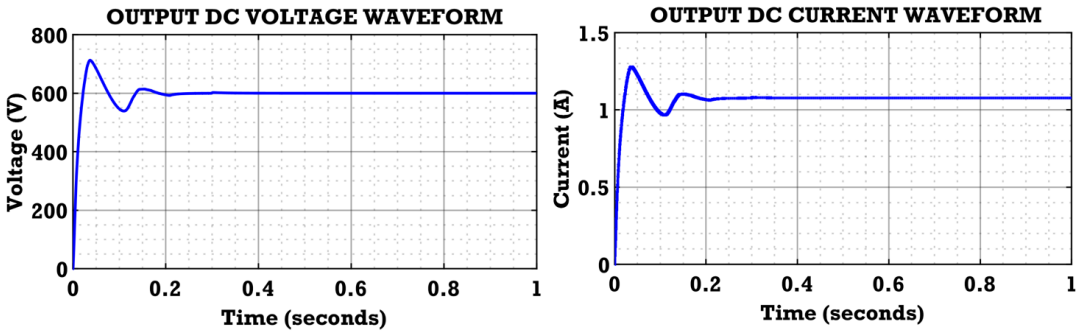

Fig. 13. Waveform of CIM converter

The waveform of CIM converter is signified in Fig. 13. Initially, the output voltage is arbitrarily altered and settled to a value of $600\ V$ in the whole system. Moreover, the output current is arbitrarily altered in starting period and continued to a value of $1.1\ A$ throughout the system.

10.22060/EEJ.2026.25521.5948

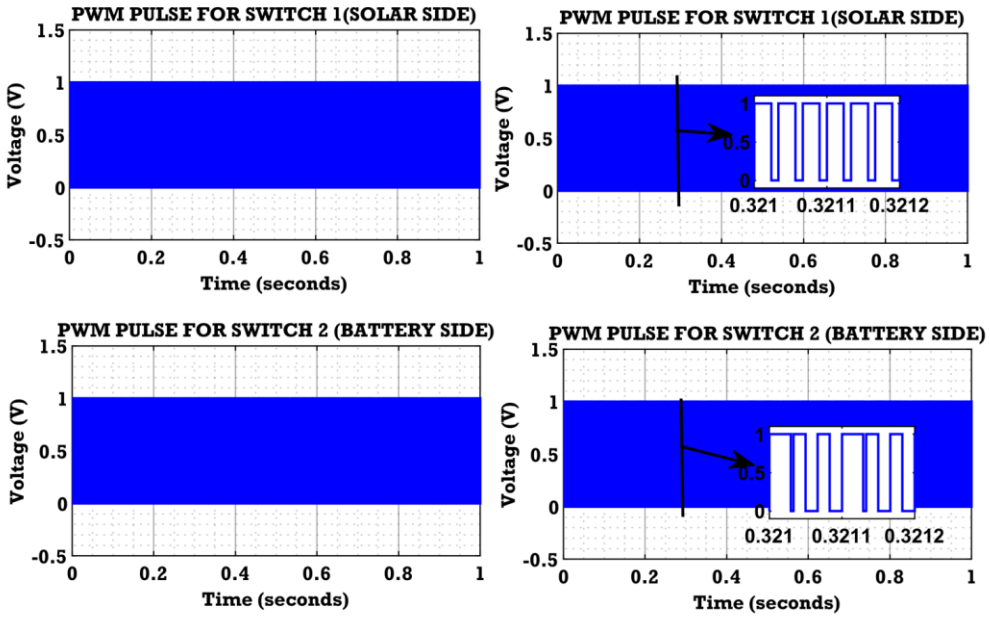

Fig. 14. Waveform of switches

The PWM pulse waveform of switches are displayed in Fig. 14. The waveform of switch 1 on solar side is varied from $0\ to\ 1\ V$ in the entire system. The PWM pulse for switch 2 on battery side is changed from $0\ to\ 1\ V$ throughout the system. The PWM pulse for switch 1 on solar side is sustained to a value of $0-1\ V$ and PWM pulse for switch 2 maintained a value of $0-1\ V$ on the whole system.

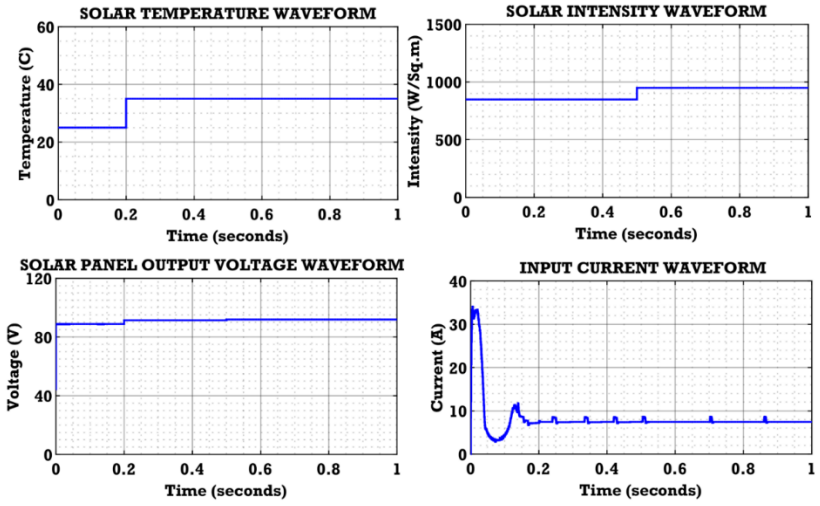

Fig. 15. Waveform of solar panel

The waveform of solar panel is displayed in Fig. 15. Here, the temperature is varied and settled at 35℃ while the intensity is steadied at $1000(W/Sq.m)$. Consequently, the current and voltage on output side are sustained at 8 A and 100 V with little fluctuations.

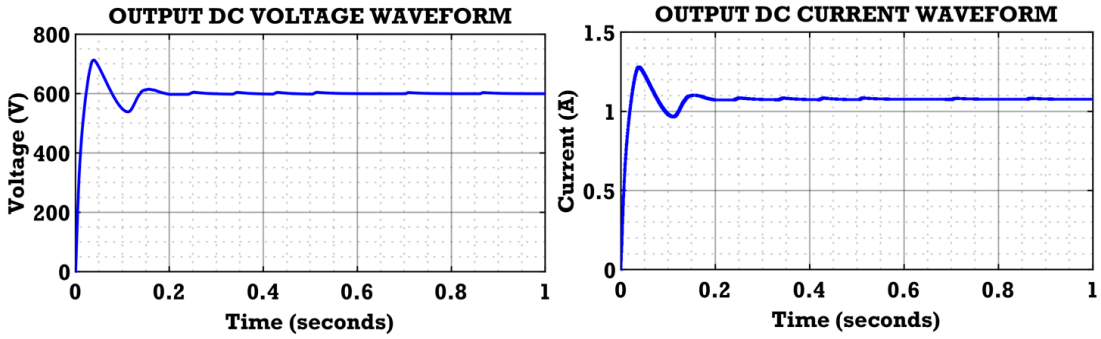

Fig. 16. Waveform of CIM converter

The current on output side is sustained at 1.1 A with voltage on output side is stabilized at 600 V throughout the system, as seen in Fig. 16.

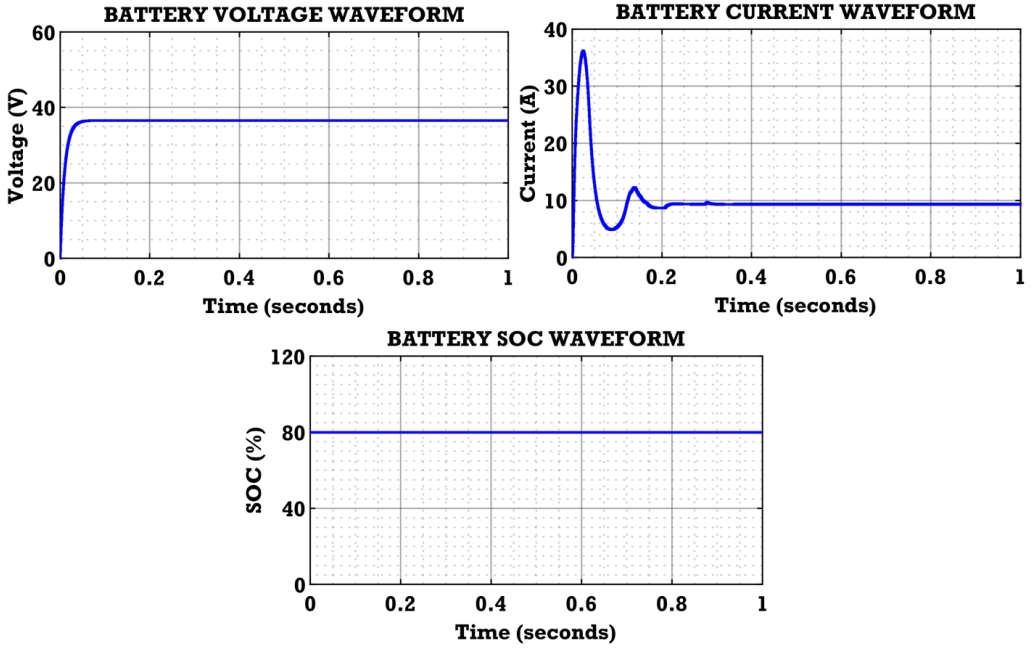

Fig. 17. Waveform of battery

10.22060/EEJ.2026.25521.5948

The waveform of battery is displayed in Fig. 17. Here, its voltage progressively elevated and continued at 35 V whereas the current is steadied at 10 A and SOC is settled at 80% in the complete system.

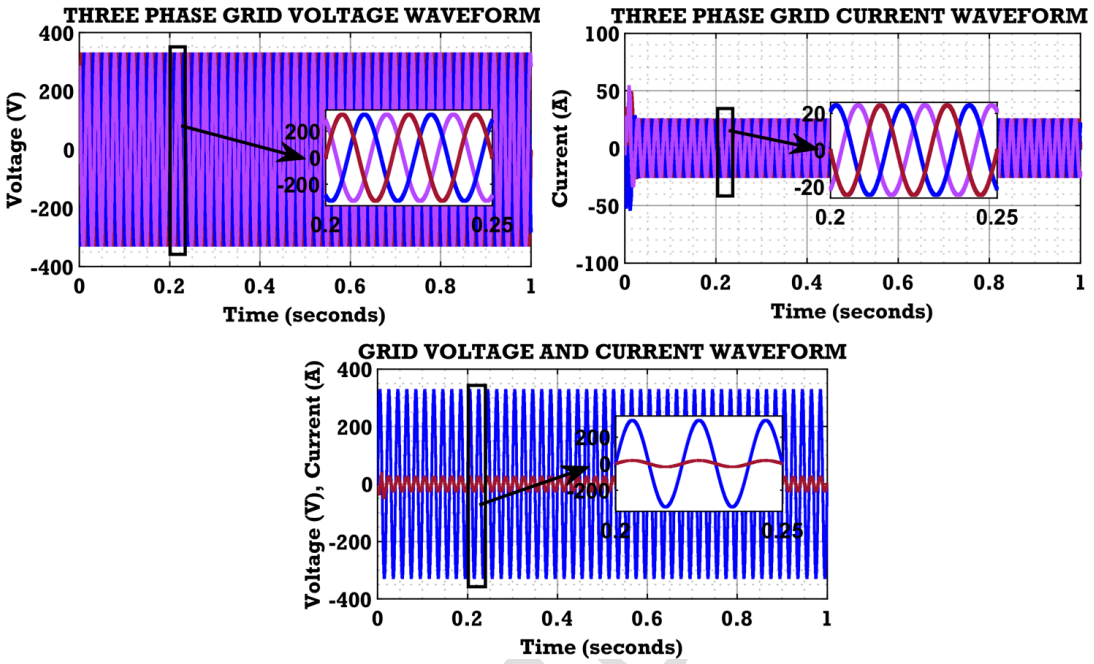

Fig. 18. Waveform of grid

Fig. 18 indicate the waveform of grid in 12 kW load condition. The grid voltage is continued to 320 V and current is continued to a value of 30 A. Inphase voltage and current is continued at 320 V, 30 A in the complete system.

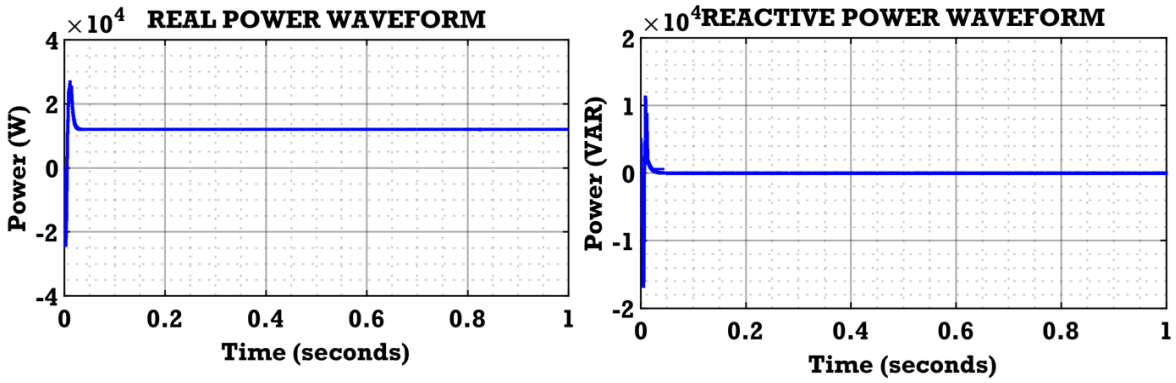

Fig. 19. Waveform of power

10.22060/EEJ.2026.25521.5948

The real and reactive power is presented in Fig. 19. The value of real and reactive power maintained a stable value in the system.

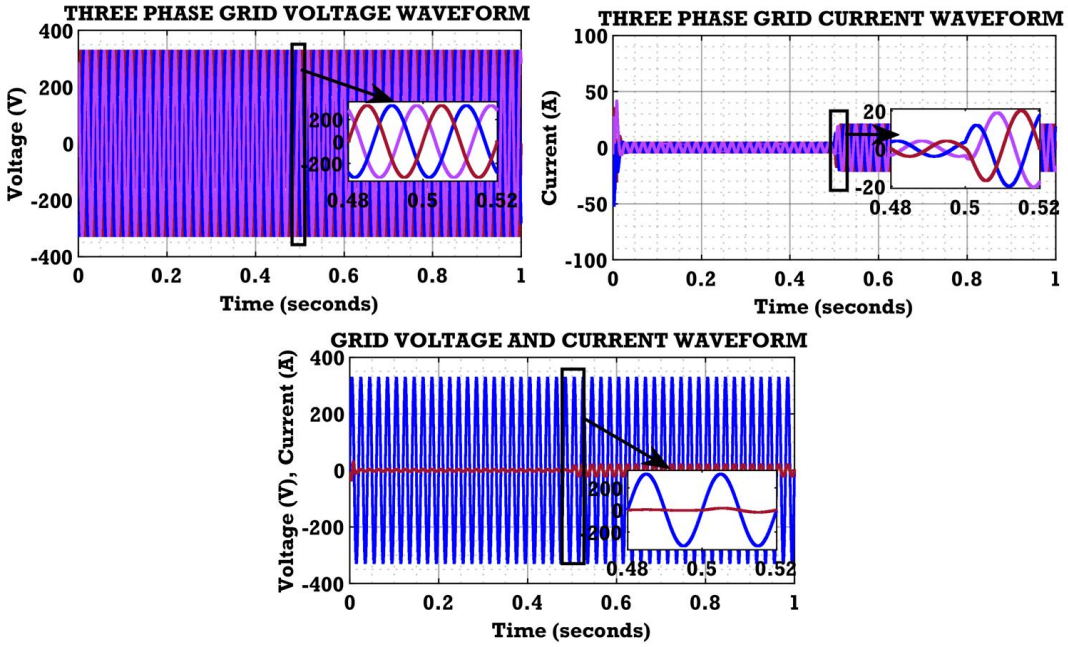

Fig. 20 Waveform of grid

The waveform of grid in 2-10 kW load circumstance is represented in Fig. 20. Here, the voltage is steadied at 320 V whereas the current is continued at 10 A and the grid voltage and current are settled at 320 V, 10 A.

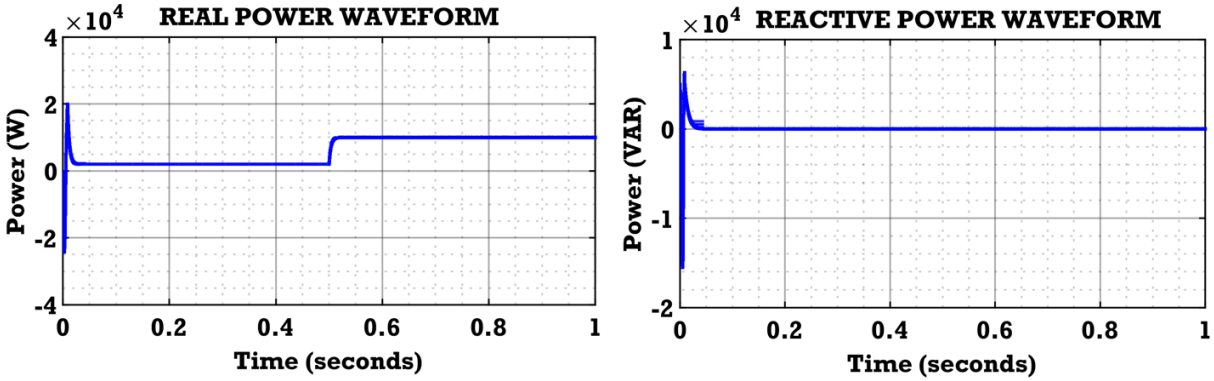

10.22060/EEJ.2026.25521.5948

Fig. 21 Waveform of power

The real power is continued at a lesser value whereas the reactive power is maintained at a smaller value, as seen in Fig.21.

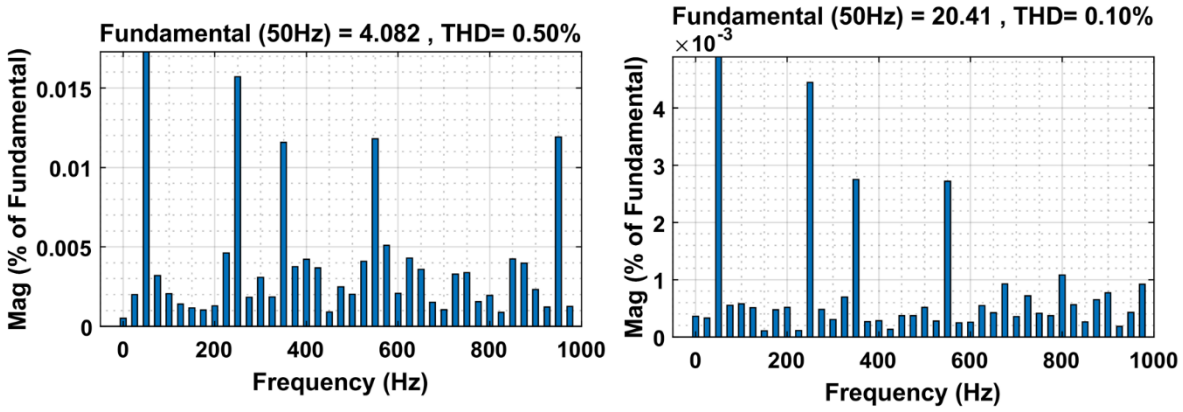

Fig. 22. THD Waveform

The THD waveform for 2 kW and 10 kW load circumstance is revealed in Fig. 22. Here, the lowermost THD of 0.1% is attained by the 10 kW load condition.

10.22060/EEJ.2026.25521.5948

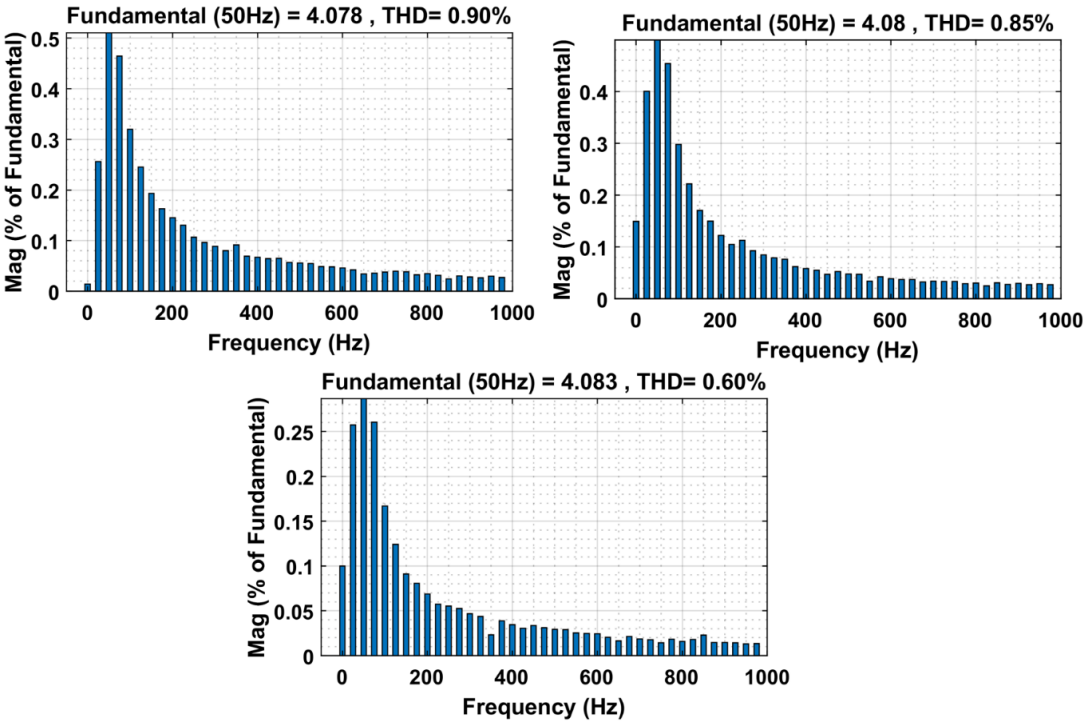

Fig. 23. Waveform of THD

Fig. 23 depicts the waveform of Total Harmonic Distortion (THD). The lowest THD value of 0.6% is attained by the B phase, thereby the harmonic distortion is reduced.

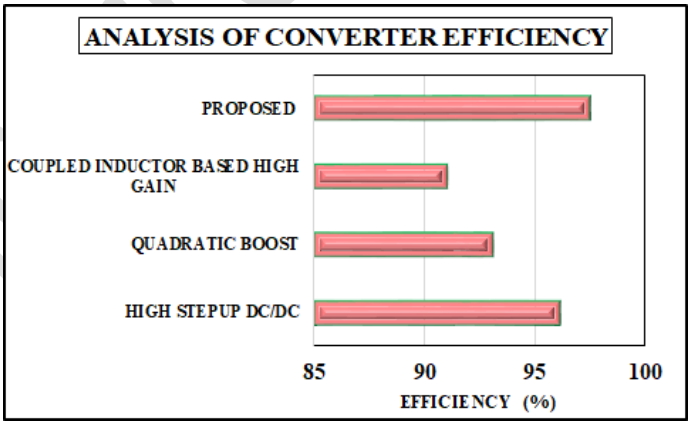

Fig. 24. Analysis of efficiency

The CIM converter has the maximum efficiency of 97.46%, indicates that there is an improvement in energy conversion compared to other approaches, as depicted in Fig. 24. The other converters like high stepup

DC/DC [23], Quadratic Boost [24], Coupled inductor based high gain [25] are attains the efficiency of 96.1%, 93.1% and 91%, representing its poorer performance in energy conversion.

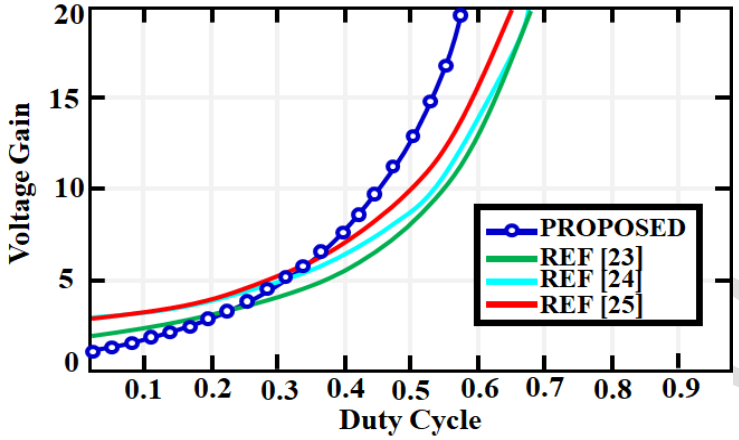

Fig. 25. Analysis of voltage gain

Fig. 25 displays the voltage gain for high stepup [23], Quadratic Boost [24], Coupled inductor based high gain [25] converter. The CIM converter attains the maximum voltage gain than other converter approaches, denotes its superiority in performance.

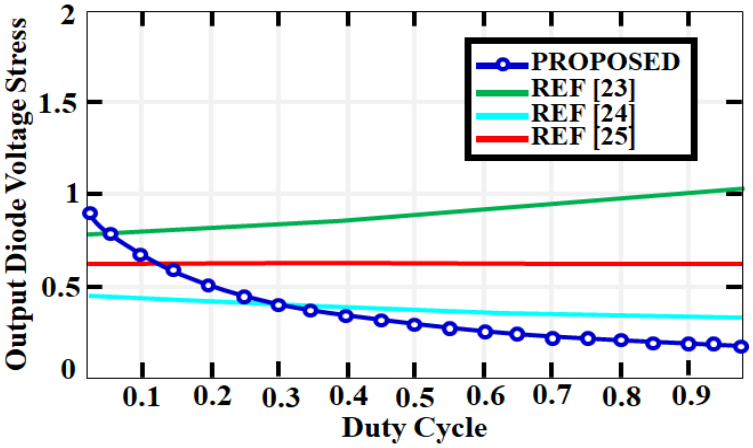

Fig. 26. Analysis of voltage stress

10.22060/EEJ.2026.25521.5948

The voltage stress on output diode with high stepup [23], Quadratic Boost [24], Coupled inductor-high gain [25] converter is indicated in Fig. 26. The low voltage stress is achieved by CIM converter that results in reduced conduction and switching losses.

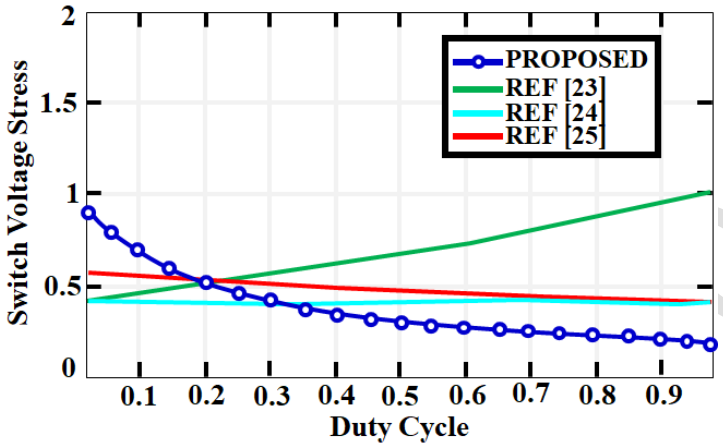

Fig. 27. Analysis of voltage stress on switch

The CIM converter attains the lowermost voltage stress on switch than other converters such as high stepup DC/DC [23], Quadratic Boost [24], Coupled inductor based high gain [25] converter, as depicted in Fig. 27.

4. Conclusion

This paper develops an integration of PV system with a CIM converter for enhanced power delivery. The use of a CIM converter, significantly maximizes the PV system's voltage. With the PI controller, the CIM converter's performance is optimized, Grid synchronization has been achieved by PI by comparing the reference and actual power values, resulting in the lowest possible THD. The inverter has maintained the standard theory levels of harmonics and power quality concerns. The overall work is verified using MATLAB/Simulink and comparison is done with conventional approaches. The results validate that the developed approach produces converter efficiency of 97.46%, assures the overall performance is enhanced.

References

[1] V. Rajagopal, D. Sharath, G. Vishwas, J. Bangarraju, S.R. Arya, and C. Venkatesh, "Optimized Controller Gains Using Grey Wolf Algorithm for Grid Tied Solar Power Generation with Improved Dynamics and Power Quality", 2022 In Chinese Journal of Electrical Engineering, vol. 8, no. 2, pp. 75-85.

[2] F. Wu, B. Yang, A. Hu, Y. Zhang, W. Ge, L. Ni, C. Wang, and Y. Zha, "Inertia and Damping Analysis of Grid-Tied Photovoltaic Power Generation System With DC Voltage Droop Control", 2021 In IEEE Access, vol. 9, pp. 38411-38418.

[3] P. Puranen, A. Kosonen, and J. Ahola, "Technical feasibility evaluation of a solar PV based off-grid domestic energy system with battery and hydrogen energy storage in northern climates", 2023 Solar Energy, vol. 213, pp. 246-259.

[4] M.M.R. Ahmed, S. Mirsaeidi, M.A. Koondhar, N. Karami, E.M. Tag-Eldin, N.A. Ghamry, R.A. EI-Sehiemy, Z.M. Alaas, I. Mahairq, and A.M. Sharaf, "Mitigating Uncertainty Problems of Renewable Energy Resources through Efficient Integration of Hybrid Solar PV/Wind Systems into Power Networks", 2024 In IEEE Access, vol. 12, pp. 30311-30328.

[5] N.C. Alluraiah, and P. Vijayapriya, "Optimization, Design, and Feasibility Analysis of a Grid-Integrated Hybrid AC/DC Microgrid System for Rural Electrification", 2023 In IEEE Access, vol. 11, pp. 67013-67029.

[6] G.M. Jagadeesan, R. Pitchaimuthu, and M. Sridharan, "A Two-stage Single-phase Grid-connected Solar-PV System with Simplified Power Regulation", 2022 In Chinese Journal of Electrical Engineering, vol. 8, no. 1, pp. 81-92.

[7] K.P. Joshua, L.V. Rangasamy, C.V.K. Reddy, and R. Veeruchinnan, "Energy management of solar photovoltaic fed water pumping system based BLDC motor drive using NBO–SDRN approach", 2024 Electrical Engineering, vol. 106, no. 3, pp. 3045-3059.

[8] K. Sarita, S. Kumar, A.S.S. Vardhan, R.M. Elavarasan, R.K. Saket, G.M. Shafiullah, and E. Hossain, "Power Enhancement With Grid Stabilization of Renewable Energy-Based Generation System Using UPQC-FLC-EVA Technique", 2020 In IEEE Access, vol. 8, pp. 207443-207464.

[9] K.S. Kavin, P. Subha Karuvelam, M. Devesh Raj, and M. Siva Subramanian, "A Novel KSK Converter with Machine Learning MPPT for PV Applications", 2024 Electric Power Components and Systems, pp. 1-19.

[10] M.M. Gulzar, A. Iqbal, D. Sibtain, and M. Khalid, "An Innovative Converterless Solar PV Control Strategy for a Grid Connected Hybrid PV/Wind/Fuel-Cell System Coupled With Battery Energy Storage", 2023 In IEEE Access, vol. 11, pp. 23245-23259.

[11] I. Akhtar, S. Kirmani, and M. Jameel, "Reliability Assessment of Power System Considering the Impact of Renewable Energy Sources Integration into Grid with Advanced Intelligent Strategies", 2021 In IEEE Access, vol. 9, pp. 32485-32497.

[12] K.Y. Yap, C.R. Sarimuthu, and J.M.Y. Lim, "Grid Integration of Solar Photovoltaic System Using Machine Learning-Based Virtual Inertia Synthetization in Synchronverter", 2020 In IEEE Access, vol. 8, pp. 49961-49976.

[13] N. Babu, J.M. Guerrero, P. Siano, R. Peesapati, and G. Panda, "An improved adaptive control strategy in grid-tied PV system with active power filter for power quality enhancement", 2020 IEEE Systems Journal, vol. 15, no. 2, pp. 2859-2870.

[14] C.M.N. Mukundan, P. Jayaprakash, U. Subramaniam, and D.J. Almakhles, "Binary Hybrid Multilevel Inverter-Based Grid Integrated Solar Energy Conversion System with Damped SOGI Control", 2020 In IEEE Access, vol. 8, pp. 37214-37228.

[15] M.M. Mabrook, A.A. Donkol, A.M. Mabrouk, A.I. Hussein, and M. Barakat, "Enhanced the Hosting Capacity of a Photovoltaic Solar System Through the Utilization of a Model Predictive Controller", 2024 In IEEE Access, vol. 12, pp. 62480-62491.

[16] U. Younas, A.A. Kulaksiz, and Z. Ali, "Deep Learning Stack LSTM Based MPPT Control of Dual Stage 100 kWp Grid-Tied Solar PV System", 2024 In IEEE Access, vol. 12, pp. 77555-77574.

[17] I. Hassan, I. Alhamrouni, Z. Younes, N.H. Azhan, S. Mekhlif, M. Seyedmahmoudian, and A. Stojcevski, "Explainable Deep Learning Model for Grid-Connected Photovoltaic System Performance Assessment for Improving System Reliability", 2024 In IEEE Access, vol. 12, pp. 120729-120746.

[18] J.E. Hernández-Díez, C.F. Méndez-Barrios, S.I. Niculescu, and E. Ernesto Bárcenas-Bárcenas, "A current sensorless delay–based control scheme for MPPT–boost converters in photovoltaic systems", 2020 IEEE Access, vol. 8, pp. 174449-174462.

[19] H.Y. Ahmed, O. Abdel-Rahim, and Z.M. Ali, "New high-gain transformerless dc/dc boost converter system", 2022 Electronics, vol. 11, no. 5, pp. 734.

[20] I. Dagal, and B. Akin, "Improved particle swarm optimization based on buck-boost converter (IPSO-BBC) for photovoltaic system applications", 2022 Recent Adv. Sci. Eng, vol. 2, no. 2, pp. 42-48.

[21] B. Chandrasekar, C. Nallaperumal, S. Padmanaban, M.S. Bhaskar, J.B. Holm-Nielsen, Z. Leonowicz, and S.O Masebinu, "Non-isolated high-gain triple port DC–DC buck-boost converter with positive output voltage for photovoltaic applications", 2020 IEEE Access, vol. 8, pp. 113649-113666.

[22] N. Priyadarshi, M.S. Bhaskar, F. Azam, M. Singh, D.K. Dhaked, I.B.M. Taha, and M.G. Hussien, "Performance evaluation of solar-PV-based non-isolated switched-inductor and switched-capacitor high-step-up cuk converter", 2022 Electronics, vol. 11, no. 9, pp. 1381.

[23] S. Hasanpour, Y.P. Siwakoti, A. Mostaan, and F. Blaabjerg, "New semi quadratic high step-up DC/DC converter for renewable energy applications", 2021 IEEE Trans. Power Electron, vol. 36, no. 1, pp. 433-446.

[24] A. Mirzaee, S. Arab Ansari, and J. Shokrollahi Moghani, "Single switch quadratic boost converter with continuous input current for high voltage applications", 2020 International Journal of Circuit Theory Application, vol. 48, no. 4, pp. 587-602.

[25] P. Upadhyay, R. Kumar, and S. Sathyan, “Coupled-inductor-based high gain converter utilising magnetising inductance to achieve soft-switching with low voltage stress on devices”, 2020 IET Power Electron, vol. 13, no. 3, pp. 576-591.